# Abundant photoelectronic behaviors of $La_{0.67}Sr_{0.33}MnO_3$/Nb:$SrTiO_3$ junctions*

Hai-Lin Huang(黄海林)[1,2], Deng-Jing Wang(王登京)[1,†], Hong-Rui Zhang(张洪瑞)[2], Hui Zhang(张慧)[2], Chang-Min Xiong(熊昌民)[3], Ji-Rong Sun(孙继荣)[2], and Bao-Gen Shen(沈保根)[2]

[1] *Department of Applied Physics, Wuhan University of Science and Technology, Wuhan* 430081, *China*
[2] *Beijing National Laboratory for Condensed Matter Physics and Institute of Physics, Chinese Academy of Sciences, Beijing* 100190, *China*
[3] *Department of Physics, Beijing Normal University, Beijing* 100875, *China*

(Received 22 March 2017; revised manuscript received 8 April 2017; published online 6 June 2017)

Temperature dependence on rectifying and photoelectronic properties of $La_{0.67}Sr_{0.33}MnO_3$/Nb:$SrTiO_3$ (LSMO/STON) junctions with the thickness values of LSMO film varying from 1 nm to 54 nm are systematically studied. As shown experimentally, the junctions exhibit good rectifying properties. The significant differences in photoemission property among the LSMO/STON junctions are observed. For the junction in a thicker LSMO film, the photocurrent shows a monotonic growth when temperature decreases from 300 K to 13 K. While for the junction in an ultrathin LSMO film, the behaviors of photocurrent are more complicated. The photocurrent increases rapidly to a maximum and then smoothly decreases with the decrease of temperature. The unusual phenomenon can be elucidated by the diffusion and recombination model of the photocarrier.

**Keywords:** manganite, heterojunction, photocurrent

**PACS:** 73.40.Lq, 75.47.Lx, 73.50.Pz **DOI:** 10.1088/1674-1056/26/7/077302

## 1. Introduction

As a typical strongly correlated electron system, the perovskite manganite oxides owning novel properties due to the coexistence of coupled charge, spin, lattice and orbital degree of freedom,[1,2] has received extensive attention. The manganite oxide film junctions usually exhibit many distinctive properties under the external field, such as bias voltage-dependent positive or negative magnetoresistance,[3–5] magnetic tunning rectification characteristics,[6] etc. Recently, photovoltaic devices based on correlated electron oxides have received increasing attention.[7–10] The photoelectronic process can be described as the photocarrier, that is, electron and hole are produced by photon, which is separated by the built-in potential at the interface of the junction, and then collected as photocurrent or photovoltage. Fruitful achievements have been obtained, such as temperature-dependent photovoltaic,[11,12] and photo induces unusual electric transport property[13] and magneto-tunable photovoltaic effect.[14]

$La_{1-x}Sr_xMnO_3$ is a prototypical manganese oxide, and only manganite whose Curie temperature ($T_C$) is above room temperature. For the $La_{1-x}Sr_xMnO_3$/Nb:$SrTiO_3$ heterojunction, more interesting, magnetic, electronic and transport properties can be quite different when the film thickness of $La_{1-x}Sr_xMnO_3$ film decreases, particular in several nanometer.[15–18] However, most of the previous studies focused on thick manganite films of junctions at room temperature. The photovoltaic effect of thin film junctions at low temperature is not very clear and deserves further study. In this report, we choose 0.05 wt% Nb-doped $SrTiO_3$ (STON) and $La_{0.67}S_{r0.33}MnO_3$(LSMO), for which the optimal doping and $T_C$ is as high as 360 K to compose the heterojunction. The values of band gap ($E_g$) of LSMO and STON are respectively $\sim$ 1 eV and $\sim$ 3.2 eV. That is, only photocarriers of LSMO could be generated by visible photon when the photon energy is 1.6–3.1 eV. In the experiments, the junctions exhibit good rectifying properties and obvious differences in dynamic photoemission properties are observed when temperature decreases from 300 K to 13 K. In the thick film of LSMO/STON junctions, the photocurrent shows a monotonic growth when temperature decreases and the change ratio of photocurrent is as high as 300%. While, in the ultrathin film of junctions, the photocurrent behaviors exhibit more complicated: first a rapid growth, then a dramatic drop with the decrease of the temperature. The same photoelectric behaviors are obtained under visible lasers with wavelengths of 532 nm and 405 nm.

## 2. Experimental procedure

A series of LSMO films was grown in-situ, via the pulsed laser deposition technique, on $TiO_2$-terminate (001)-oriented STON substrates. In the deposition process, temperature of the substrate was kept at 700 °C and the oxygen pressure at 30 Pa. After deposition, the films were cooled down to room temperature in the atmosphere of 100 Pa oxygen pressure to reduce the vacancy defects. The size of sample was $3\times5$ mm$^2$,

*Project supported by the National Natural Science Foundation of China (Grant Nos. 11520101002 and 11474024).
†Corresponding author. E-mail: wangdengjing@wust.edu.cn
 

and LSMO film thickness $t$ was controlled by the number of laser pulses, that is, $t = 1$, 3, 5, 13, 54 nm in the experiment. To reconfirm the thickness of LSMO film, x-ray reflection (XRR) analysis was also performed on a Bruker diffractometer (D8 Discover), and results were in accordance with the former results. The crystal structure of film was analyzed by x-ray diffraction (XRD). The film surface morphology was investigated by atomic force microscope (AFM). Magnetization and transport measurement were performed by a quantum designed superconducting quantum interference device magnetometer (SQUID) equipped with an electrical measurement device.

As electrodes, two Ag pads, each with a size of $1\times1$ mm$^2$, were deposited on LSMO and STON, respectively. A laser with a spot size of $\sim 2$ mm$^2$ was located at the adjacent the top electrode, and the wavelengths of 532 nm and 405 nm were used in the experiments. A Keithley Source Meter 2600 was used for data collection. The temperatures of the samples were controlled by a cycling helium cryostat with the temperatures ranging from 310 K to 13 K.

## 3. Results and discussion

The surface topographies of the LSMO films are investigated by AFM. The films are very smooth and the root-mean-square roughness vales of the films vary from 0.2–0.8 nm. Figures 1(a) and 1(b) present AFM images of the 1-nm-thick LSMO. Clearly terrace-structured surface with a height of step is $\sim 0.4$ nm is observed. Figure 1(c) shows the XRD pattern recorded around the (002) peak of the 5-nm-thick LSMO film of LSMO/STON junction. The (002) peaks of LSMO and STON are observed clearly. Both indicate high quality of the LSMO/STON junctions that we have achieved.

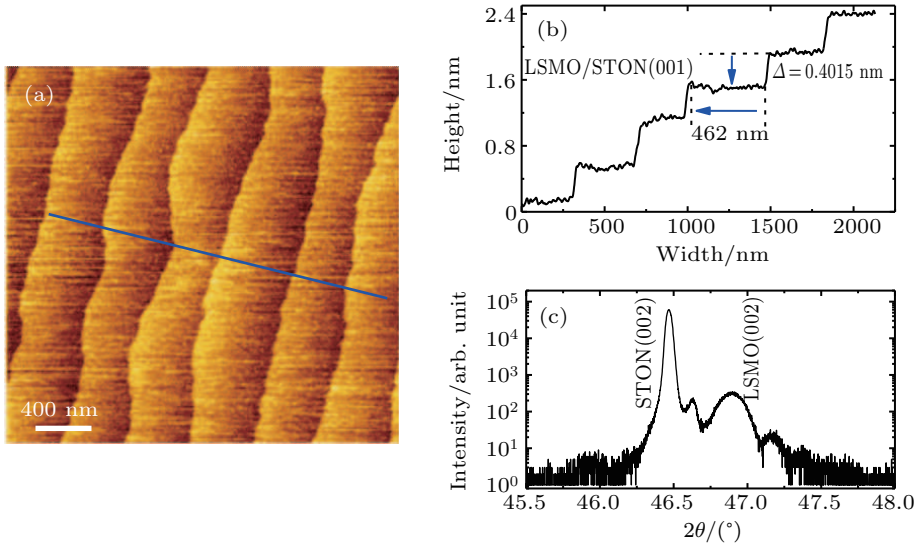


**Fig. 1.** (color online) ((a), (b)) Surface topographies of the LSMO (1 nm)/STON junction and the scale of image is $2.5\times2.5$ μm$^2$; (c) XRD spectrum of the 5-nm-thick LSMO film grown on STON.

The resistivity dependent on the temperature of the LSMO film is measured by the standard four-probe technique with an applied current of 1 μA along the manganite film plane. When the thickness of LSMO film is above 5 nm, the metal-insulator transition clearly exists. When the thickness is less than 3 nm, it exhibits insulator behavior, that is, the resistivity rapidly increases with the decrease of temperature. With the decrease of the film thickness, the Curie temperature monotonically decreases as shown in Fig. 4(b) and is consistent with the previous result.[15]

The current ($I$)–voltage ($V$) curves of the junctions are measured by using a two-probe configuration. Two Ag pads, each with a size of $1\times1$ mm$^2$, were deposited on LSMO and STON as electrodes. Appropriate electric pulses are applied to the Ag–STON and Ag–LSMO contacts to obtain an Ohmic contact. The resistance is $\sim 50$ Ω for the Ag–LSMO contact and $\sim 20$ Ω for the Ag–STON contact, and electric current flowing from LSMO to STON is defined as positive as shown in the inset of Fig. 2(a). Figure 2(a) shows the $I$–$V$ curves of LSMO/STON junctions, and the excellent rectifying behaviors indicated by strongly asymmetric $I$–$V$ curves against electric polarity are observed. The current is tiny in the zero-bias limit and remains small as the reverse bias voltage increases, whereas it grows steeply with voltage bias increasing in the forward direction. To obtain more information about junctions, a further analysis of the temperature dependence of the $I$–$V$ curves, which is expected to vary exponentially against the interfacial barrier, is required. Based on the semiconductor theory,[19] the $I$–$V$ relation of an ideal junction can be described by the formula $I \approx I_0 \exp(eV/nk_BT)$ for $eV > nk_BT$ in the forward direction. The prefactor $I_0$ is the reverse saturation current and it varies according to the relation $I_0 \propto \exp(-\phi_d/k_BT)$, where $\phi_d$ is the interfacial potential, $k_B$ is Boltzmann's constant, and $n$ is the ideality factor. Fig-

ures 2(b) and 2(c) show temperature-dependent ideality factor and interfacial barriers of LSMO/STON junctions. No obvious difference in the junction between different-thickness LSMOs is observed. The ideality factor is close to 1 at high temperature and increases slowly when the temperature decreases, which indicates that the thermoionic emission process for electronic transport is dominant. At temperatures below 100 K, ideality factor is larger than 2 and increases rapidly, which indicates that the electronic transport model transforms into quantum tunneling model. The interfacial potential $\phi_d$ decreases with decreasing temperature and the maximal $\phi_d$ is approximate to 0.8 V at room temperature. The interfacial potential of the LSMO/STON heterojunctions is consistent with that of the other manganite heterojunctions.[20] The information about junction interface can also be obtained from the capacitance ($C$)–voltage ($V$) characteristics. According to the semiconductor theory,[10,19] the formula of $C$–$V$ relation is $1/C^2 \propto (\phi_d - eV)$. We show the linearity between the inverse square of the capacitance ($C^{-2}$) and the applied voltage ($V$) of 54 nm film of LSMO/STON junction at 300 K. The value of $\phi_d$ is 0.96 eV as shown in Fig. 2(d), which is consistent with the former results.

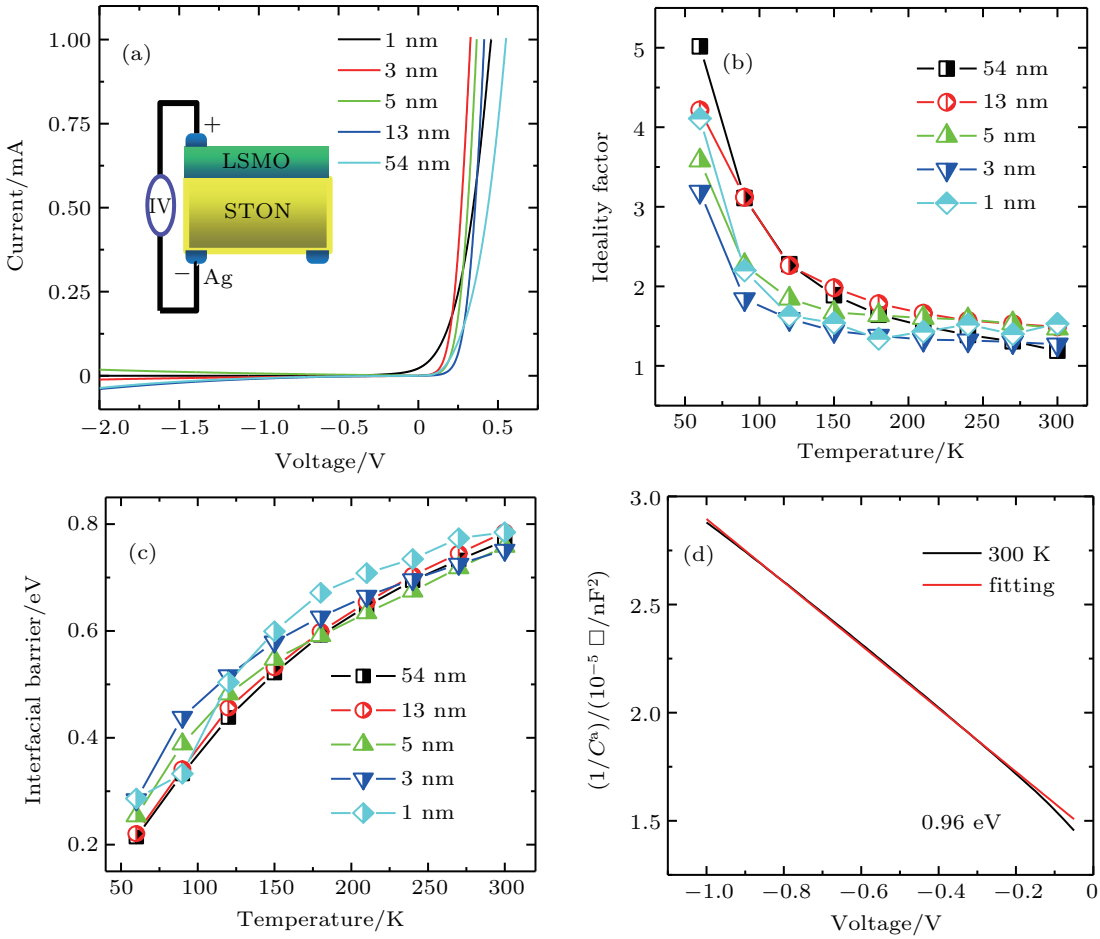


**Fig. 2.** (color online) (a) Current–voltage characteristics of LSMO/STON junctions. ((b), (c)) Ideality factor and interfacial barriers of junctions from 300 K to 50 K at 30 K intervals. (d) $1/C^2$–$V$ relations of 54 nm film of LSMO/STON junction. Solid lines are guide for eyes.

According to the photoelectric theory,[8,19] only when the photon energy $E > E_g$, can the valance electrons be activated into conduction band. That is, electrons/holes are generated by light photons. The photocarriers are separated by built-in potential at the interface of junction, and form photocurrent when short circuit happens. As discussed before, with the decrease of the film thickness of junction, the physical/chemical environments of photocarriers could be different, indicating their unique properties. Figure 3 shows the temperature-dependent photocurrent of LSMO/STON junctions under the 532 nm laser of 10 mW. We can observe that the photocurrent-temperature relations are completely different. The photocurrent increases monotonically upon cooling when the LSMO film thickness of junctions is above 5 nm. In the ultrathin film of junctions, the relations are more complicated. Taking 3 nm film of junction for example, three different processes are exhibited: with the decrease of temperature, the photocurrent increases rapidly to a maximal value, then slowly decreases, and quickly drops under the low temperature. The change ratio of photocurrent can be up to 300%. The same photoelectric behaviors are obtained by using the laser with a wavelength of 405 nm.

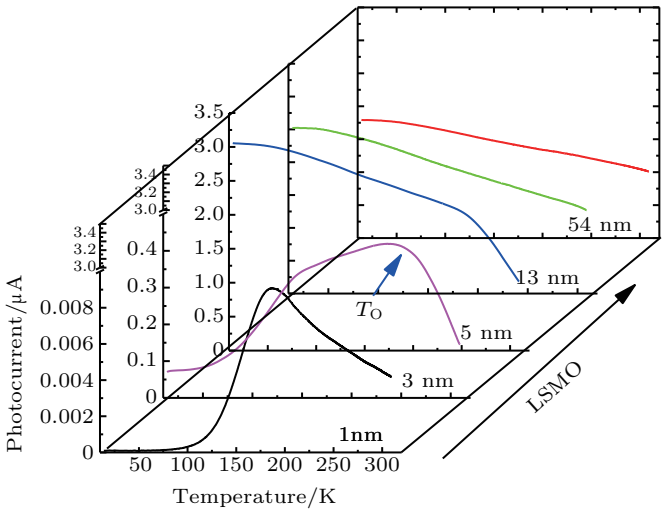


**Fig. 3.** (color online) Temperature dependence of photocurrent of LSMO/STON junctions. A 10 mW laser with a wavelength of 532 nm is used.

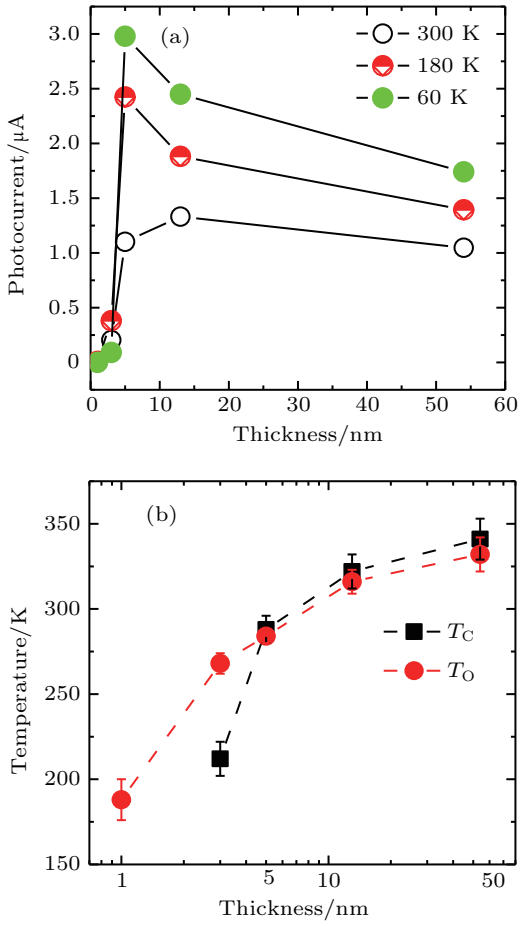


**Fig. 4.** (color online) (a) Thickness-dependent photocurrent of junctions; (b) thickness-dependent $T_O$ and $T_C$ of LSMO/STON junctions. Solid lines are guide for eyes.

Thickness dependence of photocurrent is shown in Fig. 4(a). With thickness increasing, the photocurrent dramatically increases up to a saturation value and then slowly decreases. Definite diffusion distance of the photocarriers might cause abnormal photoelectric behaviors in ultrathin film of junctions. When the diffusion distance of photocarriers is comparable to or larger than film thickness, the size effect might occur. That is, diffusion distance, mobility and lifetime of nonequilibrium carriers would be greatly reduced. Moreover, more defects and impurity energy levels in ultrathin film of junctions, which could become effective recombination center for photocarriers, influence the photocurrent of junctions.[8,17,18] Theoretical analysis reveals that the diffusion distance in the junction is only a few nanometers,[8,18] which is consistent with our experimental result. Moreover, the transition point of the photocurrent against temperature is defined as $T_O$ just as shown in Fig. 3. A comparison of $T_O$ with $T_C$ shows that $T_O$ matches well with the $T_C$ as shown in Fig. 4(b), indicating that magnetic status of films might also affect photovoltaic effect of junctions. These novel physical phenomena have not been reported before.

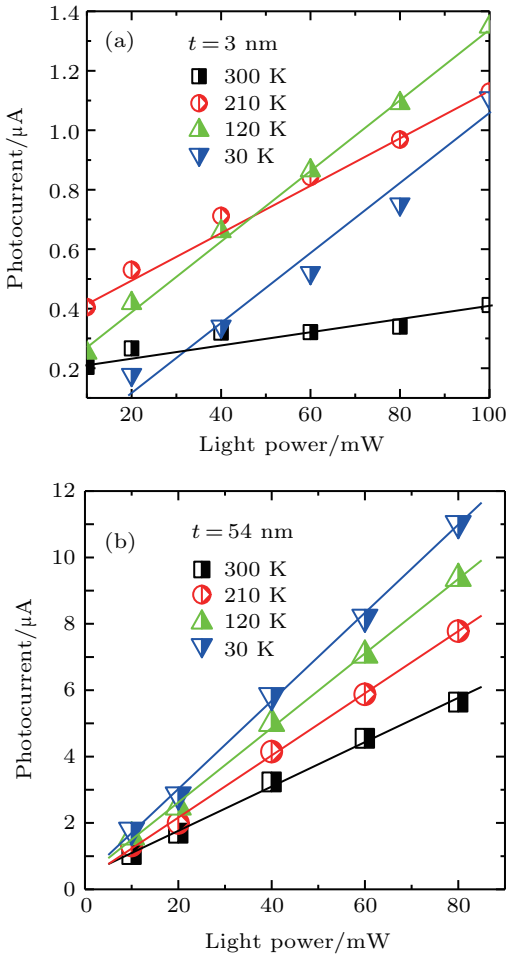


**Fig. 5.** (color online) Photocurrent-light power relations of LSMO/STON with the film thickness values of (a) 3 nm and (b) 54 nm, respectively.

Figure 5 shows the well linear relation of photocurrent with light power of the junctions, taking 3 nm and 54 nm film of junctions for example. According to the semiconductor theory,[19,21] photocurrent can be expressed as $I_{ph} = q\Delta n\mu E$, where $q$ is the electron charge, $\Delta n$ is the number of photocarriers, $\mu$ is the mobility of the photocarriers, and $E$ is the internal

electric field. To a certain junction, in which depletion layer and interfacial states are fixed, the change in $I_{ph}$ is exclusively ascribed to the change of $\Delta n$. As the irradiation power increases, more and more photons are absorbed by electrons in valence band, which leads to the fact that more photocarriers are generated and the photocurrent is linearly grown. Under different temperatures, the change of the slope indicates the diverse rates of photocarrier generation and recombination.

## 4. Summary

In this work, we systematically study the LSMO/STON junctions with the LSMO film thickness values changing from 1 nm to 54 nm. All junctions exhibit good rectifying properties, and there is no conspicuous distinction in interfacial barrier nor ideality factor among those junctions. More interesting, obvious difference between photoemission properties of the LSMO/STON junction is observed. For the junctions with thicker LSMO film, the photocurrent shows a monotonic growth when temperature decreases and the change ratio of photocurrent is as high as 300%. While, for the junction with ultrathin LSMO film, the photocurrent grows rapidly, and then dramatically drops with the decrease of the temperature. As the film thickness increases, the photocurrent of junctions increases rapidly to a maximal value and then smoothly decreases, and the same photoelectric behaviors of LSMO/STON junctions are also observed under the visible laser wavelengths of 532 nm and 405 nm. These novel photoelectronic behaviors of junctions could be properly considered in the design of the photoelectric device, even the solar cell.

## References


[1] Imada M, Fujimori A and Tokura Y 1998 *Rev. Mod. Phys.* **70** 1039
[2] Dagotto E 2005 *Science* **309** 5732
[3] Tanaka H, Zhang J and Kawai T 2001 *Phys. Rev. Lett.* **88** 027204
[4] Sun J R, Xiong C M, Zhao T Y, Zhang S Y, Chen Y F and Shen B G 2004 *Appl. Phys. Lett.* **84** 1528
[5] Jin K J, Lu H B, Zhou Q L, Zhao K, Cheng B L, Zhou Y L and Yang G Z 2005 *Phys. Rev. B* **71** 184428
[6] Wang D J, Sun J R, Xie Y W, Lü W M, Liang S, Zhao T Y and Shen B G 2007 *Appl. Phys. Lett.* **91** 062503
[7] Koshibae W, Furukawa N and Nagaosa N 2013 *Phys. Rev. B* **87** 165126
[8] Nakamura M, Sawa A, Fujioka J, Kawasaki M and Tokura Y 2010 *Phys. Rev. B* **82** 201101
[9] Nakamura M, Sawa A, Sato H, Akoh H, Kawasaki M and Tokura Y 2007 *Phys. Rev. B* **75** 155103
[10] Saucke G, Norpoth J, Jooss C, Su D and Zhu Y M 2012 *Phys. Rev. B* **85** 165315
[11] Sun J R, Xiong C M, Shen B G, Wang P Y and Weng Y X 2004 *Appl. Phys. Lett.* **84** 2611
[12] Sun J R, Shen B G, Sheng Z G and Sun Y P 2004 *Appl. Phys. Lett.* **85** 3375
[13] Koshibae W, Furukawa N and Nagaosa N 2011 *Europhys. Lett.* **94** 27003
[14] Sheng Z G, Nakamura M, Koshibae W, Makino T, Tokura Y and Kawasaki M 2014 *Nat. Comms.* **10** 1038
[15] Huijben M, Martin L W, Chu Y H, Holcomb M B, Yu P, Rijnders G, Blank D H A and Ramesh R 2008 *Phys. Rev. B* **78** 094423
[16] Moon E J, Balachandran P V, Kirby B J, Keavney D J, Schleputz C M and Karapetrova E 2014 *Nano Lett.* **10** 1021
[17] Gao W W, Sun X, Wang J, Shang D S, Shen B G and Sun J R 2011 *J. Appl. Phys.* **109** 023909
[18] Gao W W, Lu L, Sun Y P, Sun J R, Shen J, Chen R J, Chen Y F and Shen B G 2013 *J. Appl. Phys.* **113** 17D716
[19] Size M 1981 *Physics of Semiconductor Devices*, 2nd ed. (New York: Wiley)
[20] Wang D J, Sun J R, L u W M, Xie Y W, Liang S and Shen B G 2007 *J. Phys. D: Appl. Phys.* **40** 5075
[21] Simmons J G and Taylor G W 1971 *Phys. Rev. B* **2** 502